Caenorhabditis elegans BUB-3 and SAN-1/MAD3 Spindle Assembly Checkpoint Components Are Required for Genome Stability in Response to Treatment with Ionizing Radiation

Bertolini, Simone; Wang, Bin; Meier, Bettina; Hong, Ye; Gartner, Anton

Published in:
G3 : Genes, Genomes, Genetics

DOI:
10.1534/g3.117.1122

Publication date:
2017

Document Version
Peer reviewed version

G3: Genes|Genomes|Genetics Early Online, published on October 18, 2017 as doi:10.1534/g3.117.1122

Title: *C. elegans* BUB-3 and SAN-1/MAD3 Spindle Assembly Checkpoint components are required for genome stability in response to treatment with ionizing radiation.

Simone Bertolini, Bin Wang[1], Bettina Meier, Ye Hong and Anton Gartner*

School of Life Sciences, Centre for Gene Regulation and Expression, University of Dundee. DD1 5EH Dundee, UK.

[1] Current address: Center for the biological sciences and biotechnology, Guangxi Academy of Sciences, Nanning 530007, P. R. China

Running Title: IR sensitivity of *C. elegans* BUB-3.

Keywords: Ionizing radiation
Spindle Assembly Checkpoint
BUB-3, SAN-1/MAD-3
DNA damage response

*Corresponding author: Prof. Anton Gartner, School of Life Sciences, Division of Gene Regulation and Expression, University of Dundee. DD1 5EH Dow Street, Dundee, UK.
Phone: +44 1382 385809
E-mail: a.gartner@dundee.ac.uk

ABSTRACT

Relatively little is known about the crosstalk between the spindle assembly checkpoint and the DNA damage response, especially in multicellular organisms. We performed a *Caenorhabditis elegans* forward genetic screen to uncover new genes involved in the repair of DNA damage induced by ionizing radiation. We isolated a mutation, *gt2000* which confers hypersensitivity to ionizing radiation and showed that *gt2000* introduces a premature stop in *bub-3*. BUB-3 is a key component of the spindle assembly checkpoint. We provide evidence that BUB-3 acts during development and in the germline; irradiated *bub-3(gt2000)* larvae are developmentally retarded and form abnormal vulvae. Moreover, *bub-3(gt2000)* embryos sired from irradiated worms show increased levels of lethality. Both *bub-3* and *san-1* (the *Caenorhabditis elegans* homologue of MAD3) deletion alleles confer hypersensitivity to ionizing radiation, consistent with the notion that the spindle assembly checkpoint pathway is required for DNA damage response. *bub-3(gt2000)* is moderately sensitive to the crosslinking drug cisplatin but not to UV light or methyl methanesulfonate. This is consistent with role in dealing with DNA double-strand breaks and not with base damage. Double mutant analysis revealed that *bub-3* does not act within any of the three major pathways involved in the repair of double-strand breaks. Finally, the *cdc-20* gain-of-function mutant *cdc-20/fzy-1(av15),* which is refractory to the cell cycle delay conferred by the spindle checkpoint showed phenotypes similar to *bub-3* and *san-1* mutants. We speculate that BUB-3 is involved in DNA damage response through regulation of cell cycle timing.

AUTHOR SUMMARY

The spindle assembly checkpoint delays anaphase progression when chromosomes are not attached to the spindle. Following on an unbiased forward genetic screen we found the spindle assembly checkpoint components BUB-3 and SAN-1/MAD-3 are required to ensure viability after treatment with ionizing radiation. We provide evidence the spindle checkpoint is required during somatic development and in germ cells. Furthermore, we find that BUB-3 and SAN-1/MAD-3 act independently of the DNA repair pathways known to mend double-strand breaks caused by ionizing irradiation, possibly by changing cell cycle timing during development.

INTRODUCTION

Faithful DNA replication and chromosome segregation are essential for maintaining genome integrity. To ensure the high fidelity of these processes checkpoint mechanisms have evolved to delay cell cycle progression when DNA damage is sensed or chromosome alignment is incomplete. The DNA damage checkpoint senses DNA lesions using the ATM and ATR apical sensors to affect transient cell cycle arrest and efficient DNA repair. In contrast, the spindle assembly checkpoint (SAC) was classically implicated in delaying anaphase onset until all mitotic chromosomes are aligned at the mitotic spindle. Failure to do so can leads to chromosome missegregation and ensuing aneuploidy. It was established that the SAC delays progression to anaphase when chromosomes are not attached to the kinetochore by inhibiting the Cdc20/FZY-1 activator of the Anaphase Promoting Complex (APC) (HWANG *et al.* 1998). The APC is

an E3 ubiquitin ligase that triggers anaphase by inducing the degradation of cyclin B and securin. The latter protein binds to and thereby inhibits separase, a protease that allows for the separation of chromatids by cohesin cleavage. Current models posit that three conserved SAC proteins (Mad2, Bub3 and Mad3/BubR1) interact with each other to generate the Mitotic Checkpoint Complex (MCC) that is responsible for Cdc20/FZY-1 inhibition (MUSACCHIO AND SALMON 2007; LARA-GONZALEZ *et al.* 2012; PRIMORAC AND MUSACCHIO 2013). The SAC protein Mad2 adopts two native conformations, namely the 'open' (O-Mad2) and 'closed' (C-Mad2) state. According to the 'Mad2 template model' (DE ANTONI *et al.* 2005), Mad2 exists as the inactive diffusible O-Mad2 conformer when kinetochores are correctly attached to the spindle. In presence of unbound kinetochores, a fraction of Mad2 proteins adopts the C-Mad2 active state to form a tetrameric 2:2 complex with Mad1 on the unattached kinetochores. Mad1-bound C-Mad2 recruits O-Mad2 at the unattached kinetochore to facilitate the interaction between O-Mad2 and Cdc20/FZY-1. Upon binding to Cdc20/FZY-1 O-Mad2 then switches conformation to the C-Mad2 state. The C-Mad2:Cdc20 complex is then released to the cytoplasm and leads to the inhibition of the APC (MUSACCHIO AND SALMON 2007). In parallel to Mad2 activation, Bub3 and Mad3/BubR1 form a dimer that binds to C-Mad2:Cdc20, thereby assembling the MCC (ESSEX *et al.* 2009). The active MCC persists until all chromosomes have achieved bipolar attachment to the mitotic spindle. Once this is achieved, the MCC is disassembled and Cdc20/FZY-1 promotes anaphase by activating the APC. In addition to the function in checkpoint signaling, Bub3 was recently shown to promote metaphase to anaphase transition in the absence of spindle perturbation (KIM *et al.* 2015).

Although the SAC is active at low levels in unperturbed S-phase to ensure timely onset of mitosis (MAGIERA *et al.* 2014), it is not essential for the growth of haploid budding yeast cells in the absence of spindle perturbation. Components of the spindle assembly checkpoint were initially found in genetic screens for mutants that bypass the mitotic cell cycle arrest phenotype conferred by the microtubule poisons nocodazole and benomyl (HOYT *et al.* 1991; LI AND MURRAY 1991). In contrast to haploid yeast, most homologues of the SAC genes are required for viability in animals even in absence of spindle damage (GORBSKY *et al.* 1998; WILD *et al.* 2016). This is thought to be due to the role of the SAC in delaying anaphase onset (WILD *et al.* 2016). Indeed, the delay of anaphase onset by the SAC is also required for ordered segregation of chromosomes during the first meiotic division in budding yeast (SHONN *et al.* 2000). In mouse, MAD2 deficiency does not allow embryos to develop beyond the E6.5 stage (DOBLES *et al.* 2000). In *C. elegans*, depletion of BUB-1 by RNAi causes high levels of embryonic lethality (TARAILO *et al.* 2007). Loss-of-function *mdf-1*$^{\text{MAD-1}}$ mutants display severe defects during larval development that prevent strain propagation (KITAGAWA AND ROSE 1999; STEIN *et al.* 2007). Similarly, loss of MAD-2 results in low brood size, reduced progeny viability and high frequency of larval defects (KITAGAWA AND ROSE 1999; STEIN *et al.* 2007). In contrast, BUB-3 and MAD-3 appear to be dispensable for survival under physiological conditions in *C. elegans* (NYSTUL *et al.* 2003; TARAILO *et al.* 2007; HAJERI *et al.* 2008).

Several lines of evidence indicate that SAC and DNA damage response (DDR) have overlapping functions. Although SAC was initially believed not to participate in DDR (HOYT *et al.* 1991; HARDWICK *et al.* 1999), it was later shown that Mad1p and Mad2p contribute to the pre-anaphase arrest induced by DNA replication defects and the

DNA-damaging agent methyl methanesulfonate (MMS) in budding yeast (GARBER AND RINE 2002; PALOU *et al.* 2017). It was hypothesized that damaged centromeric DNA disrupts the structure of kinetochores and, as a result, altered kinetochores elicit the SAC-dependent cell cycle arrest. However, the role of kinetochores in DNA damage-induced cell cycle arrest has been called into question as mutants that lack kinetochores are still capable of sustaining a durable arrest in the presence of DNA damage (KIM AND BURKE 2008). Nevertheless, a clear role for the centromere in the DNA damage response has been established in *S. cerevisiae* when a double-strand break (DSB) is induced within 100,000 base pairs distance to the centromere (DOTIWALA *et al.* 2010). The full cell cycle arrest conferred by this persistent DSB is dependent on the SAC and the DNA damage checkpoint pathways and requires histone modifications at centromeric DNA (DOTIWALA *et al.* 2010). It was suggested that a DSB close to a centromere leads to altered chromatin conformation that triggers kinetochore dysfunction recognized by the SAC (DOTIWALA *et al.* 2010). Another role for spindle assembly checkpoint proteins appears to be to confer efficient cell cycle arrest when ssDNA is enriched at subtelomeric regions upon depletion of the nonhomologous end joining DNA repair factor yKu70Δ in *S. cerevisiae* (MARINGELE AND LYDALL 2002). It was suggested that chromosome fusions occurring in yKu70Δ mutants lead to the formation of dicentric chromosomes, which have previously been shown to trigger the spindle assembly checkpoint (NEFF AND BURKE 1992). Crosstalk between DNA damage checkpoint and the SAC appears to be conserved from yeast to humans. p53-deficient cancer cells treated with DNA polymerase inhibitor aphidicolin elicit a BubR1-dependent metaphase arrest (NITTA *et al.* 2004). Similar observations were obtained from a study in murine fibroblasts (FANG *et al.* 2006).

Interestingly, some *C. elegans sac* mutants show persistent DNA double-strand breaks upon exposure to ionising radiation (IR) and upon hydroxyurea (HU) treatment, which blocks DNA replication (LAWRENCE *et al.* 2015). These DNA-damaging agents induce MAD-2 to co-localise with damaged DNA at the nuclear periphery of proliferating germ cells in interphase. Peripheral localization of MAD-2 is dependent on the DNA damage response kinase ATR. These results are in line with the DNA damage-induced cell cycle arrest phenotype being alleviated in *mad-2* mutants and MAD-2 possibly also playing a direct role in DSB repair at the nuclear periphery (LAWRENCE *et al.* 2015).

In this study, we isolated a *C. elegans* strain that carries a mutation in the SAC gene *bub-3* using a forward genetic approach. *bub-3* mutants are hypersensitive when exposed to ionizing radiation and to the DNA crosslinking agent cisplatin. Epistasis analysis suggests that *bub-3* acts independently of the major DNA repair pathways involved in DNA double-strand break repair. Moreover, the characterization of a *cdc-20* gain-of-function allele, *fzy-1(av15),* suggests that SAC proteins might have a role in regulating cell cycle timing in response to DNA damage.

MATERIAL AND METHODS

***C. elegans* strains and maintenance:** *C. elegans* strains were maintained at 20°C on *E. coli* OP-50 seeded NGM agar plates as described previously (BRENNER 1974). The N2 Bristol reference line TG1813 is used in the Gartner laboratory as the wild-type reference strain. All mutant strains were outcrossed six times to TG1813 except *bub-3 (gt2000),* which was outcrossed 3 times to TG2435. Strains used in this paper are: TG1813 N2

Bristol, TG2435 *vtIs1[pdat-1::gfp; rol-6] V*, CB4856 Hawaii, TG3796 *bub-3(gt2000) II*, RB1391 *san-1(ok1580) I*, VC2773 *bub-3(ok3437) II*, TG1660 *xpf-1(tm2842) II*, DW102 *brc-1(tm1145) III*, RB873 *lig-4(ok716) III*, TG2534 *polq-1(tm2026) III*, RB2422 *polh-1(ok3317) III*, TG1540 *gen-1(tm2940) III*, TG3899 *bub-3(gt2000) II; brc-1(tm1145) III*, TG3870 *bub-3(gt2000) II; polq-1(tm2026) III*, TG3900 *bub-3(gt2000) II; lig-4(ok716) III*, TG4071 *fzy-1(av15) II*, TG4085 *fzy-1(av15) bub-3(gt2000) II*, TG4092 *cop1146[Pbub-3::eGFP*::*bub-3::3'UTRbub-3*], TG4193 *cop1146[Pbub-3::eGFP*::*bub-3::3'UTRbub-3*]; *odIs57[Ppie-1::mCherry::histoneH2B + unc-119(+)]*; *unc-119(ed3)*, TG4196 *odIs57[Ppie-1::mCherry::histoneH2B + unc-119(+)]*; *ItIs38[pie-1::GFP::PH(PLC1delta1) + unc-119(+)]; unc-119(ed3)*, TG4197 *odIs57[Ppie-1::mCherry::histoneH2B + unc-119(+)]*; *ItIs38[pie-1::GFP::PH(PLC1delta1) + unc-119(+)]; unc-119(ed3); bub-3(gt2000) II*. The *cop1146[Pbub-3::eGFP*::*bub-3::3'UTRbub-3]* eGFP insertion was generated by Knudra (http://www.knudra.com/) following the procedures described in DICKINSON *et al.* 2015. Exact details are available upon request.

Mutagenesis screen and mutation identification: Mutagenesis and screening procedures were performed as described in GONZALEZ-HUICI *et al.* 2017. SNP mapping was performed according to the protocol described in DAVIS *et al.* 2005. For whole-genome sequencing, genomic DNA was extracted and purified using ChargeSwitch® gDNA mini tissue kit (Invitrogen) and sent to GenePool (http://genepool.bio.ed.ac.uk/) for Illumina (Solexa) sequencing. Paired-end sequencing was set to achieve 24X coverage (100 bp paired-end reads for a total of 24,000,000 reads). Quality of the reads was checked using FastQC. Reads were then aligned to the *C. elegans* reference genome

(WBcel235.74) using BWA mem. Variants in the strains TG1813 and TG2435 were called using the software SAMtools and Bfctools. Heterozygous variants and variants that were not unique to the mutant strain were filtered out. We then extracted homozygous variants within the 900 kb region determined by SNP mapping. Homozygous unique variants were then ranked based on the severity of the predicted effect on the genome. The *gt2000* mutation was supported by 18 sequence reads including reads from both directions, confirmed visually using IGV software.

Sensitivity assays: For L1 sensitivity assay, gravid adults were bleached and eggs were incubated at 20º under shaking for at least 13 hours to obtain synchronised populations of L1 larvae. Larvae were plated on seeded NGM plates and irradiated at the indicated doses using a 137Cs source (IBL 437C, CIS Bio International). Animals that developed into L4 larvae within 49 hours post-irradiation were scored as well as the total number of plated larvae. Ruptured worms were scored 72 hours post-irradiation as percentage of total number of plated worms. For IR and UV treatments of young adults, animals were irradiated at the indicated doses. After 24 hours one worm was singled out on a plate, to allow for egg-laying for 12 hours. The adult was then removed and the number of laid eggs was scored. The number of dead (unhatched eggs) embryos was scored 24 hours after removal of the adult. A minimum of 6 plates per condition was analyzed. For genotoxin treatment, young adults were incubated in liquid solution (M9 buffer [3 g/l KH2PO4, 6 g/l Na2HPO4, 5 g/l NaCl, 1 mM MgSO4] + OP50 + genotoxins at indicate concentration) at 20º under shaking for 16 hours. After incubation, worms were washed with fresh M9 buffer and transferred onto seeded NGM plates for 24 hours to recover before being transferred again in freshly seeded NGM plates for 6 hours to lay eggs (3

worms per plate for a total of 3 plates per condition). The number of laid eggs was scored immediately after removal of adults. Dead eggs were scored 24 hours after removal of adults. For irradiation of late stage embryos, we followed the protocol described in CLEJAN *et al.* 2006.

DAPI- and immuno-staining: DAPI staining of oocytes and RAD-51 immunostaining was performed as described in GONZALEZ-HUICI *et al.* 2017. For DAPI staining of whole germlines, we used a procedure described in CRAIG *et al.* 2012. For phosphoCDK-1^{Tyr15} immunostaining, we followed the protocol described in MOSER *et al.* 2009. Anti RAD-51 antibody was diluted 1:800 whereas anti phosphoCDK-1^{Tyr15} antibody was diluted to 1:100. Secondary antibody (donkey anti-rabbit conjugated with Alexa Fluor® 568, ThermoFischer Scientific) was diluted to 1:750 and to 1:1000 for RAD-51 and phosphoCDK-1^{Tyr15} immunostaining, respectively. DeltaVision wide-field microscope with Coolsnap HQ camera and softWoRx software was used to acquire fluorescence images. To analyze and process images, we used softWoRx and Adobe® Photoshop software.

Time-lapse live embryo imaging: For time-lapse imaging of live embryos, we followed an imaging procedure as described in SONNEVILLE *et al.* 2015. Young adults were irradiated as described in the embryonic lethality assay. One-cell embryos were dissected in M9 buffer 24 hours post-irradiation and immediately mounted on 2% agarose pads. Images were acquired every 10 seconds using a spinning-disk confocal microscope (IX81; Olympus) with spinning-disk head (CSU-X1; Yokogawa Electric Corporation) and MetaMorph software (Molecular Devices). For image processing, we used the ImageJ software.

Data availability statement: *bub-3* and *mad-3* mutant strains were sent to the GCG *C. elegans* strain collection. Other strains are available upon request.

RESULTS

To uncover new genes involved in DNA damage response, we performed an unbiased forward genetic screen. Upon ethyl methanesulphonate (EMS) mutagenesis of P0 wild-type (N2) individuals, F2 animals were singled in 96-well plates (GONZALEZ-HUICI *et al.* 2017). Progeny of singled L4 stages animals was split into aliquots (GONZALEZ-HUICI *et al.* 2017). One aliquot of L1 larvae was treated with 60Gy of IR, a mutagenic agent that leads to a wide spectrum of DNA lesions including DNA double-strand breaks. The other aliquot was kept untreated to recover mutants. We selected lines that failed to propagate when subjected to IR, while propagating normally without IR treatment. IR treatment with 60 Gy does not cause a significant impairment of reproduction of the wild-type N2 strain (data not shown, Figure 1A). Here we describe a recessive mutation (*gt2000*) that shows reduced proliferation after being irradiated at the L1 stage, to an extent similar to the previously described *tm2940* mutant in the *gen-1* Holliday Junction resolvase (BAILLY *et al.* 2010) (Figure 1A). *gt2000* was outcrossed three times to reduced the number of mutations caused by EMS. *gt2000* was then mapped by using a combination of whole-genome sequencing and single nucleotide polymorphism (SNP) mapping which takes advantage of sequence polymorphisms between the wild-type N2 strain and a polymorphic strain initially isolated in Hawaii (DAVIS *et al.* 2005). The SNP mapping procedure allowed to narrow down a ~900 kbp region on chromosome II that

was likely to contain the phenotype-causing mutation (Figure 1B). In parallel, whole genome sequencing analysis of the mutant strain revealed a single base substitution in this genomic region, a C>T transition leading to a nonsense mutation in the *bub-3* gene (Figure 1C). *gt2000* introduces a stop codon at amino acid 104 truncating the last 239 amino acids of BUB-3. To further ascertain that *gt2000* is indeed the phenotype-causing mutation, we also analyzed the *bub-3*(*ok3437)* deletion allele provided by the Oklahoma knockout consortium (CONSORTIUM 2012). We found that *bub-3(ok3437)* and *bub-3(gt2000)* L1 larvae are equally sensitive to IR (Figure 1A) further confirming that *bub-3* inactivation leads to increased IR sensitivity.

BUB-3 and MAD-3 appear to be the only components of the SAC pathway not needed for survival under physiological conditions (NYSTUL *et al.* 2003; TARAILO *et al.* 2007; HAJERI *et al.* 2008). To test if the SAC pathway is generally needed for the response to DNA damage, we wondered whether mutants in *san-1*, the *C. elegans* homologue of MAD3, are equally hypersensitive to IR. We found that proliferation of *san-1(ok1580)* animals was equally delayed as in *bub-3* mutants upon IR treatment (Figure 1A). We generated a N-terminal GFP::BUB-3 translational fusion by genome editing in the *bub-3* genomic locus (Material and Methods). This fusion protein exhibited intermediate IR hypersensitivity at 60 Gy compared to *bub-3* mutants, consistent with a compromised function of this fusion (Figure S1A). As expected, we observed GFP::BUB-3 on the metaphase plate along holocentric chromosomes, slowly fading away in anaphase (Figure S1B). When chromatin bridges induced by IR occur these were coated by BUB-3 consistent with *C. elegans* chromosomes being holocentric (Figure S1C). Induction of BUB-3 foci upon IR treatment was not observed (data not shown).

We next wished to determine the nature of the IR sensitivity phenotype, and to test if *bub-3* mutants are also sensitive to other DNA-damaging agents. The impairment of proliferation upon IR treatment could be due to various defects including a developmental delay, a high mortality of the treated animals, a reduced brood size and increased embryonic lethality. To assay the pace of development we irradiated L1 larvae, and allowed them to grow for ~44 hours such that 100% of wild-type N2 worms developed into the L4 stage (Figure 2A). We found *bub-3* and *san-1* mutants displayed a moderate developmental delay (also known as GRO phenotype) compared to wild-type following irradiation (Figure 2A). Furthermore, we noticed a high incidence of ruptured mutant animals whose internal tissues extruded from the vulva, a condition that ultimately leads the animals to die prematurely (RUP phenotype, Figure 2B). Several rounds of postembryonic cell divisions are required for the proper formation of the vulva, and if the vulva does not from properly due to cell division defects worms rupture, with the germline protruding through the defective vulva (RUP phenotype) (O'CONNELL *et al.* 1998). At 90 Gy, RUP worms in *bub-3(ok3437)* and in wild-type seem to occur at similar frequency. However, these results are skewed by the strong GRO phenotype in *bub-3(ok3437)* thus allowing less worms of the total number plated to develop to a stage at which the ruptured phenotype becomes evident.

In addition, we found that the lethality of embryos laid ~24 hours after irradiation of young adult stage worms was increased in *bub-3* and *san-1* mutants as compared to wild-type, albeit to a lesser extent than *brc-1* mutants, which are defective for homologous recombination (Figure 2C). This later sensitivity assay is known to reflect the sensitivity of meiotic germ cells, which develop into embryos 24 hours later

(GARTNER *et al.* 2004; CRITTENDEN *et al.* 2006; JARAMILLO-LAMBERT *et al.* 2007; CRAIG *et al.* 2012). Although the predominant type of IR-induced DNA lesion causing lethality are thought to be DNA double-strand breaks, radiation treatment can also inflict various types of secondary DNA lesions including single-strand breaks, base damage and DNA-protein crosslinks (CADET *et al.* 2004). We thus treated wild-type and *bub-3* mutants with a variety of DNA-damaging agents. UV light leads to the formation of cyclobutane pyrimidine dimers and 6,4-photoproducts. Cisplatin is a DNA crosslinking agent widely used as a chemotherapeutic agent. Besides base adducts, cisplatin forms covalent bonds linking adjacent bases (intra-strand crosslinks) and bases on opposite strands (inter-strand crosslinks), with the former type of DNA damage occurring more frequently than the latter (LEMAIRE *et al.* 1991). Methyl methanesulfonate (MMS) is an alkylating agent that leads to variety of modified bases including N7-methylguanine, N3-methyladenine and O6-methylguanine (BERANEK 1990). Although MMS has been considered a radiomimetic compound for long (CHLEBOWICZ AND JACHYMCZYK 1979; UI *et al.* 2005), it is now widely accepted that MMS provokes formation of double-strand breaks when a replicative fork encounters alkylated bases (PAQUES AND HABER 1999; HOLWAY *et al.* 2006). We found that *bub-3(gt2000)* mutants do not show increased embryonic lethality when exposed to UV light and to MMS (Figure 2D-E). However, *bub-3* mutants are moderately sensitive to cisplatin (Figure 2F). Our data indicate that *bub-3* mutants are not hypersensitive towards agents that predominately cause base changes. The intermediate sensitivity to cisplatin may reflect the sensitivity towards DNA crosslinking agents, or reduced DSB repair, DSBs being generated as intermediates during DNA crosslink repair (SCHARER 2005).

We next wished to determine the defect that causes the radiation sensitivity of *sac* mutants. When mitotic *C. elegans* germ cells are subjected to DNA damage a transient G2 cell cycle arrest occurs, a phenotype thought to allow for efficient repair before cells divide (GARTNER *et al.* 2000; MOSER *et al.* 2009). As a consequence of cell cycle arrest, the nuclei of proliferating germ cells increase their volume as cells continue to grow without dividing (GARTNER *et al.* 2000). Thus, cell density of the mitotic region can be used as readout for DNA damage-induced checkpoint activation (GARTNER *et al.* 2000). We hypothesized that the SAC pathway might regulate DNA damage-induced cell cycle arrest. L4 larvae were irradiated and germlines were dissected eight hours later. Germ cells residing in a given volume of the mitotic region were counted. As expected, cell density decreased proportionally to the intensity of the radiation treatment in wild-type whereas such reduction was not observed in the loss of function *gen-1(tm2940)* mutant, which served as a positive control (Figure 3A-B). GEN-1 is a Holliday Junction resolvase also needed for efficient checkpoint signalling (BAILLY *et al.* 2010). We could not detect a significant difference between the IR-induced cell cycle arrest in wild-type and *bub-3(gt2000)* mutants consistent with the notion that BUB-3 is not required for checkpoint signalling. Normal IR-induced G2 cell cycle arrest was confirmed by staining for the phosphotyrosine 15 residue of CDK-1, which is an established marker of the G2 cell cycle stage (MOSER *et al.* 2009) (Figure S2). We conclude that *bub-3* does not affect DNA damage-induced G2 cell cycle arrest of mitotic germ cells.

We next wished to determine if IR-induced DSBs persist in *bub-3* mutants. It has been shown that chromosomes at the diakinesis stage are fragmented in various DSB repair and checkpoint mutants when examined 48 hours after irradiation (BAILLY *et al.* 2010;

356 CRAIG *et al.* 2012). Diakinesis chromosomes are condensed and the six *C. elegans*
357 chromosomes are readily cytologically visible in oocytes just before fertilization. As
358 expected, we observed six DAPI-stained chromosomes in wild-type, *gen*-1 and *bub-3*
359 mutants when worms were not treated with IR (Figure 3C-D). Chromosome
360 fragmentation of *gen-1* became apparent upon irradiation with 60 Gy of IR as described
361 previously (BAILLY *et al.* 2010) (Figure 3C-D). In contrast, six intact chromosomes could
362 be observed in wild-type and *bub-3(gt2000)* (Figure 3C-D). While a low level of
363 fragmentation was evident in *bub-3* mutants upon treatment with 120 Gy of IR, this was
364 not increased compared to wild-type. (Figure 3C-D). We next compared the kinetics of
365 RAD-51 foci formation upon IR in wild-type and *bub-3* mutants. RAD-51 is a
366 recombinase that coats single-stranded DNA resulting from DSB processing. The number
367 and kinetics of RAD-51 foci allows for estimating repair kinetics. Typically, 12 hours
368 after treatment with 30 Gy only ~50% of mitotic germ cell nuclei contain repair foci,
369 while after 16 hours foci can only be detected in a small proportion of nuclei. We found
370 that in both wild-type and *bub-3* mutant ~50% of nuclei contained repair foci after 12
371 hours, while the percentage of nuclei with RAD-51 foci dropped to ~10% after 28 hours
372 in both genotypes (Figure S3A-B).

373 Given that there is no overt change in DSB repair kinetics in *bub-3* mutants, we
374 wondered if BUB-3 might act together with any of the known DSB repair pathways or
375 not. Repairing of DNA double-strand breaks relies at least on three major DNA repair
376 pathways, homologous recombination (HR), nonhomologous end joining (NHEJ), and
377 microhomology-mediated end joining (MMEJ). HR is a largely error free DNA repair
378 modality involving the BRCA1 protein (BRC-1 in *C. elegans*) (BOULTON *et al.* 2004;

ADAMO *et al.* 2008). NHEJ is potentially error prone and involves the direct religation of DSBs conferred by the DNA Ligase 4 protein (LIG-4 in *C. elegans*). In *C. elegans*, end joining is the major DSB repair modality in somatic tissues (CLEJAN *et al.* 2006). MMEJ is an error-prone DNA repair pathway in which blunt DNA ends are resected and scanned for microhomology recognized by polymerase θ (POLQ-1 in *C. elegans*) and used to prime DNA synthesis to fill the gaps (ROERINK *et al.* 2014; VAN SCHENDEL *et al.* 2016). We thus generated *bub-3* double mutants with *brc-1, lig-4,* and *polq-1* known to be required for HR, NHEJ and MMEJ, respectively. We analysed single and double mutants by irradiating young adults and quantifying the extent of embryonic lethality. As previously reported, *brc-1* and *polq-1* single mutants were hypersensitive to IR (Figure 4A-B) (BOULTON *et al.* 2004; MUZZINI *et al.* 2008). Interestingly, both *bub-3;polq-1* and *bub-3;brc-1* double mutants were more sensitive to IR as compared to the respective single mutants (Figure 4A-B) consistent with *bub-3* functioning in parallel to HR and MMEJ. Given that it acts predominantly in somatic cells, NHEJ is commonly assayed by measuring the growth delay of irradiated late-stage embryos. Scoring the percentage of embryos reaching the L4 stage ~48 hours after irradiation we found that both single mutants showed retarded development, the phenotype being stronger in *lig-4* mutants upon treatment with high doses of irradiation. The growth delay of *bub-3;lig-4* double mutant was dramatically increased consistent with a role of BUB-3 in somatic tissues in parallel to NHEJ (Figure 4C-D). In summary we provide genetic evidence that the SAC pathway acts independently of the known DSB repair pathways.

It is established that the SAC delays progression to anaphase by inhibiting the Cdc20/FZY-1 activator of the Anaphase Promoting Complex (APC) (HWANG *et al.*

1998). We considered the possibility that precocious entry into M-phase in *bub-3* and *mad-3* mutants might contribute to the increased sensitivity towards IR. A CDC-20 gain-of-function allele, *fzy-1(av15),* which leads to precocious M-phase entry is available (STEIN *et al.* 2007; LAWRENCE *et al.* 2015). Consistent with the role of precocious M-phase entry playing a role in conferring IR sensitivity we found that treatment of both *bub-3* and *fzy-1(av15)* mutants lead to a heightened sensitivity to IR based on developmental delay phenotypes and based on the increased incidence of the ruptured vulva phenotype (Figure 5A-C). We observed an even stronger phenotype when both mutants were combined. We investigated if treatment of *bub-3* mutants leads to precocious cell cycle progression in one- and two-cell stage embryos, but could not find evidence for this (Figure S4). However, it is known that checkpoint regulation is weak in rapidly dividing *C. elegans* embryonic cells (HOLWAY *et al.* 2006), and we thus assume that a change in cell cycle timing might occur during later cell divisions leading to the slow growth and rupture phenotypes.

DISCUSSION

In this study, we isolated a mutation (*gt2000*) from a forward genetic screen that confers hypersensitivity to IR. We found that *gt2000* leads to a premature stop codon in *bub-3*, and that the *bub-3*(*ok3437*) deletion allele similarly confers hypersensitivity to IR. Irradiation of *bub-3(gt2000)* L1 larvae induces development defects such as a developmental delay and a ruptured vulva phenotype. Moreover, irradiation of *bub-3(gt2000)* young adults increases the lethality in embryos derived from those

424 animals. *san-1*(*ok1580*) mutants are also hypersensitive to IR, consistent with the notion
425 that the SAC pathway might be activated when DNA damage is inflicted. Treatment with
426 a panel of DNA-damaging agents indicates that the SAC pathway might be required to
427 mend DSBs, while not being required for the repair of damaged DNA bases.

428 SAC components BUB-3 and SAN-1 are not essential for viability under unperturbed
429 growth conditions and the corresponding mutants do not show an overt developmental
430 phenotype (NYSTUL *et al.* 2003; TARAILO *et al.* 2007; HAJERI *et al.* 2008, and our data).
431 The spindle assembly checkpoint is composed of two branches both contributing to APC
432 inactivation by CDC20 binding (ESSEX *et al.* 2009). The Mad2 conformational change
433 needed for Cdc20 binding and inhibition is facilitated by the C-Mad2:Mad1 complex
434 linked to unattached kinetochores. In contrast Bub3 interacts with Mad3 to then bind to
435 the inhibitory C-Mad2:Cdc20 complex (ESSEX *et al.* 2009). Components of this latter
436 pathway are not needed for viability. The stronger phenotype observed in *fzy-1(av15)*
437 *bub-3(gt2000)* double mutant as compared to the two single mutants may be explained by
438 the fact that *fzy-1(av15)* is a gain of function allele; gain of function being ascribed to
439 reduced MAD-2 binding to FZY-1/CDC20, thus causing precocious cell cycle
440 progression (STEIN *et al.* 2007; LAWRENCE *et al.* 2015). The *mad-2* deletion phenotype is
441 stronger than the *bub-3* phenotype, the former leading to lethality, while overt *bub-3*
442 phenotypes are only evident upon treatment with agents such as ionizing radiation. Thus,
443 precocious cell cycle progression might be stronger when *fzy-1(av15)* and a *bub-3(null)*
444 allele are combined.
445 Our data are consistent with the SAC acting in response to DNA damage both during
446 germ cell development and during somatic development. DSB repair is predominantly

ascribed to HR and MMEJ in the germline, while NHEJ acts in somatic cells. Our double mutant analysis indicates that BUB-3 might act independently of HR, MMEJ and NHEJ pathways. It remains to be determined how BUB-3 and SAN-1/MAD-3 prevent hypersensitivity to IR. It could be possible that these two proteins directly act as DSB repair factors. Consistently, previous findings showed that MAD-2 co-localizes with RAD-51 foci at the nuclear periphery in a DDR-dependent fashion (LAWRENCE *et al.* 2015). Moreover, lack of MAD-1, MAD-2, SAN-1/MAD-3 and BUB-3 renders *C. elegans* mitotically dividing germ cells unable to process DNA damage efficiently (LAWRENCE *et al.* 2015). We could not observe any difference between wild-type and *bub-3* mutants in the number of RAD-51 foci and IR-induced chromosome fragments. It was shown that BUB-3 affects repair of HU-induced DNA damage to a lesser extent than the MAD proteins (LAWRENCE *et al.* 2015). Thus, our data are compatible with *bub-3* not affecting the kinetics of RAD-51 unloading. It has been previously shown in yeast that the function of the kinetochore is perturbed when double-strand breaks are induced in close proximity leading to spindle assembly checkpoint activation (DOTIWALA *et al.* 2010). Given the holocentric nature of *C. elegans* chromosomes, we cannot rule out this possibility. Finally, we entertain the possibility that the BUB-3 and SAN-1 branch of the spindle assembly checkpoint pathway may confer hypersensitivity to ionizing radiation by causing precocious entry into mitosis. This would be consistent with the IR sensitivity of the *fzy-1(av15)* gain of function allele previously shown to advance entry into mitosis. We investigated this hypothesis in early embryos, a system amenable for precisely measuring cell cycle timing. While we observed that cell cycle timing is extended when embryos are treated with ionizing radiation, no difference between wild-type and *bub-3*

mutant embryos could be detected. Nevertheless, checkpoint phenotypes tend to be very weak during early embryogenesis (HOLWAY *et al.* 2006) and we thus postulate that precocious entry into mitosis during development could contribute to the IR sensitivity of *bub-3* and *san-1* mutants. In summary we found that *C. elegans bub-3* and *san-1* mutants are hypersensitive to IR.

FUNDING SOURCES

This work was funded by a Wellcome Trust Programme grant to AG (0909444/Z/09/Z), together with infrastructure funding from a Wellcome Trust Strategic award (097045/B/11/Z). We acknowledge the Dundee Imaging Facility, which is supported by the Wellcome Trust Technology Platform award (097945/B/11/Z) and the MRC Next Generation Optical Microscopy award (MR/K015869/1). BW and YH were also supported by ISSF funding from the Wellcome Trust. SB was supported by a BBSRC EASTBIO PhD studentship.

CONTRIBUTIONS

SB formulated research questions and hypothesis in collaboration with BW and AG. SB applied statistical analysis to the data. BM performed bioinformatic analysis of the whole-genome sequencing data. SB performed and collected data from most of the experiments. BW performed and collected data from the genetic screen. YH helped with

real time imaging. AG and SB are responsible for data management and maintenance. SB wrote the initial draft in collaboration with AG. AG reviewed the manuscript in collaboration with SB. AG supervised the project, coordinated the research activity and acquired the financial support leading to this publication.

ACKNOWLEDGMENTS

Some strains were provided by the CGC (*Caenorhabditis* Genetics Centre), which is funded by NIH Office of Research Infrastructure Programs (P40 OD010440).

FIGURE LEGENDS

FIGURE 1. ***sac* mutants are hypersensitive to IR.** (A) Representative images of NGM plates 5 days after irradiation of L1 larvae. Wild-type animals irradiated with 60 Gy propagated normally whereas *sac* mutants *bub-3* and *san-1* showed impaired growth similar to *gen-1(tm2940)*. (B) Schematic of the SNP mapping. The horizontal bars represent the right arm of chromosome II in 20 IR sensitive F2 lines derived from a cross between CB4856 (Hawaii) and the IR sensitive mutant. Black segments identify genomic regions that contain N2 SNPs. Yellow segments correspond to genomic regions that contain Hawaiian SNPs. Vertical dashed lines show the genetic position of the indicated SNPs. *gt2000* was mapped between F14D4 and K09E4 on the physical map (top line) to a ~900 kb region that shows only N2 SNPs in all F2 lines. (C) Schematic of the exon-intron structure of *bub-3* with the location of *ok3437* deletion and *gt2000* point mutation indicated (top panel). DNA sequence surrounding the *gt2000* allele in wild-type and *bub-3(gt2000)* including the corresponding amino acid sequence is shown. The C>T

substitution in *bub-3(gt2000)*, which causes a premature stop codon is indicated by a red arrow.

FIGURE 2. **Hypersensitivity of *sac* mutants to DNA-damaging agents.** (A) Quantification of the GRO phenotype in N2, *bub-3(gt2000)*, *bub-3(ok3437)* and *san-1(ok1580)* strains treated with the indicated doses of IR. The GRO phenotype was calculated as the percentage of L1 larvae that reached the L4 stage 49 hours after irradiation. (B) Quantification of the RUP phenotype in N2, *bub-3(gt2000)*, *bub-3(ok3437)* and *san-1(ok1580)* strains. The RUP phenotype is calculated as the percentage of animals that showed ruptured vulva 72 hours after irradiation. In A and B triplicates of 100 worms each were scored for each condition. (C) Embryonic lethality of N2, *bub-3(gt2000)*, *bub-3(ok3437)* and *san-1(ok1580)* strains upon irradiation. Young adults were treated with IR at indicated doses and embryonic survival was scored as described in Materials and Methods. (D-F) Sensitivity of *polh-1(ok3317)* and *bub-3(gt2000)* to UV light (D) and MMS (E), and *xpf-1(tm2842)* and *bub-3(gt2000)* to cisplatin (F) measured by embryonic lethality. Error bars indicate SEM.

FIGURE 3. **Absence of cell cycle arrest and chromosome fragmentation phenotypes in *bub-3* mutants.** (A) Representative images of DAPI-stained mitotic germ cells of N2, *gen-1(tm2940)* and *bub-3(gt2000)* strains irradiated at the specified doses and DAPI stained 8 hours after irradiation of L4 staged larvae. (B) Boxplot showing the number of mitotic germ cells observed in N2, *gen-1(tm2940)* and *bub-3(gt2000)* strains 8 hours after

irradiation. After image acquisition, germ cells residing in a defined volume of the distal most region of the germline were scored. A minimum of 7 germlines per IR dose was analyzed. (C) Representative images of DAPI-stained bodies in oocytes of N2, *gen-1(tm2940), bub-3(gt2000)* strains irradiated with the specified doses and imaged 48 hours after IR. (D) Boxplot showing the number of DAPI-stained bodies in oocytes. A minimum of 12 oocytes per condition was analyzed.

FIGURE 4. **Epistasis analysis of *bub-3* with the main DSB repair pathways.** (A) Embryonic lethality of *bub-3(gt2000), brc-1(tm1145)* single and *bub-3(gt2000);brc-1(tm1145)* double mutants in response to IR. Worms were treated with IR at the L4 stage. (B) Embryonic lethality of *bub-3(gt2000), polq-1(tm1145)* single and *bub3(gt2000);polq-1(tm1145)* double mutants in response to IR. (C) Developmental delay of N2, *bub-3(gt2000), lig-4(ok716)* and *bub-3(gt2000); lig-4(ok716)* strains upon irradiation of late stage embryos. Late stage embryos were irradiated and allowed to hatch and to develop. Developmental delay was quantified as the percentage of embryos that developed into L4 larvae 48 hours after irradiation. Error bars indicate SEM. (D) Representative images of NGM plates 6 days after irradiation of late stage embryos.

FIGURE 5. ***fzy-1(av15)* mutants are hypersensitive to IR.** (A) Quantification of the GRO phenotype in N2, *bub-3(gt2000), fzy-1(av15)* single and *fzy-1(av15) bub-3(gt2000)* double mutants after irradiation of L1 larvae at the indicated doses. (B) Quantification of the RUP phenotype in N2, *bub-3(gt2000), fzy-1(av15)* single and *fzy-1(av15) bub-*

3(gt2000) double mutants after irradiation of L1 larvae at the indicated doses. Error bars indicate SEM. (C) Representative images of NGM plates 5 days after irradiation of late stage embryos.

FIGURE S1. (A) Embryonic lethality of N2, *bub-3(gt2000)*, GFP::BUB-3 strains after irradiation at the specified doses. (B) GFP::BUB-3 and mCherry::H2B localization in one-cell embryo at mitotic prophase, metaphase, anaphase and telophase. (C) Time-lapse images of an irradiated one-cell embryo showing GFP::BUB-3 localization on lagging chromosome during late anaphase/early telophase.

FIGURE S2. PhosphoCDK-1^{Tyr15} immunostaining of N2, *gen-1(tm2940)* and *bub-3(gt2000)* germlines (mitotic region) 8 hours after irradiation of L4 larvae.

FIGURE S3. (A) RAD-51 immunostaining in N2 and *bub-3(gt2000)* germlines (mitotic region) 12 hrs and 26 hrs post-irradiation with 30 Gy. (B) Boxplot showing the percentage of RAD-51 positive mitotic germ cells in N2 and *bub-3(gt2000)* strains 12 and 26 hours after irradiation of young adults with 30 Gy. n = 13, 9, 23, 6 germlines analyzed for N2 (12 hrs), N2 (26 hrs), *bub-3(gt2000)* (12 hrs) and *bub-3(gt2000)* (26 hrs), respectively.

FIGURE S4. Barplot showing the time taken from anaphase onset in P0 (one-cell embryo) to anaphase onset in the P1 cell (two-cell embryo) in N2 and *bub-3(gt2000)* without irradiation and following irradiation with 120 Gy. n = 6, 6, 6, 3 germlines analyzed for N2 (0 Gy), N2 (120 Gy), *bub-3(gt2000)* (0 Gy), *bub-3(gt2000)* (120 Gy), respectively. Error bars indicate SEM.

REFERENCES

Adamo, A., P. Montemauri, N. Silva, J. D. Ward, S. J. Boulton *et al.*, 2008 BRC-1 acts in the inter-sister pathway of meiotic double-strand break repair. EMBO Rep 9**:** 287-292.

Bailly, A. P., A. Freeman, J. Hall, A. C. Declais, A. Alpi *et al.*, 2010 The Caenorhabditis elegans homolog of Gen1/Yen1 resolvases links DNA damage signaling to DNA double-strand break repair. PLoS Genet 6**:** e1001025.

Beranek, D. T., 1990 Distribution of methyl and ethyl adducts following alkylation with monofunctional alkylating agents. Mutat Res 231**:** 11-30.

Boulton, S. J., J. S. Martin, J. Polanowska, D. E. Hill, A. Gartner *et al.*, 2004 BRCA1/BARD1 orthologs required for DNA repair in Caenorhabditis elegans. Curr Biol 14**:** 33-39.

Brenner, S., 1974 The genetics of Caenorhabditis elegans. Genetics 77**:** 71-94.

Cadet, J., S. Bellon, T. Douki, S. Frelon, D. Gasparutto *et al.*, 2004 Radiation-induced DNA damage: formation, measurement, and biochemical features. J Environ Pathol Toxicol Oncol 23**:** 33-43.

599 Chlebowicz, E., and W. J. Jachymczyk, 1979 Repair of MMS-induced DNA double-
600 strand breaks in haploid cells of Saccharomyces cerevisiae, which requires the
601 presence of a duplicate genome. Mol Gen Genet 167**:** 279-286.
602 Clejan, I., J. Boerckel and S. Ahmed, 2006 Developmental modulation of
603 nonhomologous end joining in Caenorhabditis elegans. Genetics 173**:** 1301-1317.
604 Consortium, C. e. D. M., 2012 Large-scale screening for targeted knockouts in the
605 Caenorhabditis elegans genome. G3 (Bethesda) 2**:** 1415-1425.
606 Craig, A. L., S. C. Moser, A. P. Bailly and A. Gartner, 2012 Methods for studying the
607 DNA damage response in the Caenorhabdatis elegans germ line. Methods in cell
608 biology 107**:** 321-352.
609 Crittenden, S. L., K. A. Leonhard, D. T. Byrd and J. Kimble, 2006 Cellular analyses of
610 the mitotic region in the Caenorhabditis elegans adult germ line. Mol Biol Cell
611 17**:** 3051-3061.
612 Davis, M. W., M. Hammarlund, T. Harrach, P. Hullett, S. Olsen *et al.*, 2005 Rapid single
613 nucleotide polymorphism mapping in C. elegans. BMC genomics 6**:** 118.
614 De Antoni, A., C. G. Pearson, D. Cimini, J. C. Canman, V. Sala *et al.*, 2005 The
615 Mad1/Mad2 complex as a template for Mad2 activation in the spindle assembly
616 checkpoint. Curr Biol 15**:** 214-225.
617 Dickinson, D. J., A. M. Pani, J. K. Heppert, C. D. Higgins and B. Goldstein, 2015
618 Streamlined Genome Engineering with a Self-Excising Drug Selection Cassette.
619 Genetics 200**:** 1035-1049.

620 Dobles, M., V. Liberal, M. L. Scott, R. Benezra and P. K. Sorger, 2000 Chromosome
621 missegregation and apoptosis in mice lacking the mitotic checkpoint protein
622 Mad2. Cell 101**:** 635-645.
623 Dotiwala, F., J. C. Harrison, S. Jain, N. Sugawara and J. E. Haber, 2010 Mad2 prolongs
624 DNA damage checkpoint arrest caused by a double-strand break via a
625 centromere-dependent mechanism. Curr Biol 20**:** 328-332.
626 Essex, A., A. Dammermann, L. Lewellyn, K. Oegema and A. Desai, 2009 Systematic
627 analysis in Caenorhabditis elegans reveals that the spindle checkpoint is
628 composed of two largely independent branches. Mol Biol Cell 20**:** 1252-1267.
629 Fang, Y., T. Liu, X. Wang, Y. M. Yang, H. Deng *et al.*, 2006 BubR1 is involved in
630 regulation of DNA damage responses. Oncogene 25**:** 3598-3605.
631 Garber, P. M., and J. Rine, 2002 Overlapping roles of the spindle assembly and DNA
632 damage checkpoints in the cell-cycle response to altered chromosomes in
633 Saccharomyces cerevisiae. Genetics 161**:** 521-534.
634 Gartner, A., A. J. MacQueen and A. M. Villeneuve, 2004 Methods for analyzing
635 checkpoint responses in Caenorhabditis elegans. Methods Mol Biol 280**:** 257-274.
636 Gartner, A., S. Milstein, S. Ahmed, J. Hodgkin and M. O. Hengartner, 2000 A conserved
637 checkpoint pathway mediates DNA damage--induced apoptosis and cell cycle
638 arrest in C. elegans. Molecular cell 5**:** 435-443.
639 Gonzalez-Huici, V., B. Wang and A. Gartner, 2017 A Role for the Nonsense-Mediated
640 mRNA Decay Pathway in Maintaining Genome Stability in Caenorhabditis
641 elegans. Genetics.

642 Gorbsky, G. J., R. H. Chen and A. W. Murray, 1998 Microinjection of antibody to Mad2
643 protein into mammalian cells in mitosis induces premature anaphase. J Cell Biol
644 141**:** 1193-1205.
645 Hajeri, V. A., A. M. Stewart, L. L. Moore and P. A. Padilla, 2008 Genetic analysis of the
646 spindle checkpoint genes san-1, mdf-2, bub-3 and the CENP-F homologues hcp-1
647 and hcp-2 in Caenorhabditis elegans. Cell Div 3**:** 6.
648 Hardwick, K. G., R. Li, C. Mistrot, R. H. Chen, P. Dann *et al.*, 1999 Lesions in many
649 different spindle components activate the spindle checkpoint in the budding yeast
650 Saccharomyces cerevisiae. Genetics 152**:** 509-518.
651 Holway, A. H., S. H. Kim, A. La Volpe and W. M. Michael, 2006 Checkpoint silencing
652 during the DNA damage response in Caenorhabditis elegans embryos. J Cell Biol
653 172**:** 999-1008.
654 Hoyt, M. A., L. Totis and B. T. Roberts, 1991 S. cerevisiae genes required for cell cycle
655 arrest in response to loss of microtubule function. Cell 66**:** 507-517.
656 Hwang, L. H., L. F. Lau, D. L. Smith, C. A. Mistrot, K. G. Hardwick *et al.*, 1998
657 Budding yeast Cdc20: a target of the spindle checkpoint. Science 279**:** 1041-1044.
658 Jaramillo-Lambert, A., M. Ellefson, A. M. Villeneuve and J. Engebrecht, 2007
659 Differential timing of S phases, X chromosome replication, and meiotic prophase
660 in the C. elegans germ line. Dev Biol 308**:** 206-221.
661 Kim, E. M., and D. J. Burke, 2008 DNA damage activates the SAC in an ATM/ATR-
662 dependent manner, independently of the kinetochore. PLoS Genet 4**:** e1000015.

663 Kim, T., M. W. Moyle, P. Lara-Gonzalez, C. De Groot, K. Oegema *et al.*, 2015
664 Kinetochore-localized BUB-1/BUB-3 complex promotes anaphase onset in C.
665 elegans. J Cell Biol 209**:** 507-517.
666 Kitagawa, R., and A. M. Rose, 1999 Components of the spindle-assembly checkpoint are
667 essential in Caenorhabditis elegans. Nat Cell Biol 1**:** 514-521.
668 Lara-Gonzalez, P., F. G. Westhorpe and S. S. Taylor, 2012 The spindle assembly
669 checkpoint. Curr Biol 22**:** R966-980.
670 Lawrence, K. S., T. Chau and J. Engebrecht, 2015 DNA Damage Response and Spindle
671 Assembly Checkpoint Function throughout the Cell Cycle to Ensure Genomic
672 Integrity. PLoS Genet 11**:** e1005150.
673 Lemaire, M. A., A. Schwartz, A. R. Rahmouni and M. Leng, 1991 Interstrand cross-links
674 are preferentially formed at the d(GC) sites in the reaction between cis-
675 diamminedichloroplatinum (II) and DNA. Proc Natl Acad Sci U S A 88**:** 1982-
676 1985.
677 Li, R., and A. W. Murray, 1991 Feedback control of mitosis in budding yeast. Cell 66**:**
678 519-531.
679 Magiera, M. M., E. Gueydon and E. Schwob, 2014 DNA replication and spindle
680 checkpoints cooperate during S phase to delay mitosis and preserve genome
681 integrity. J Cell Biol 204**:** 165-175.
682 Maringele, L., and D. Lydall, 2002 EXO1-dependent single-stranded DNA at telomeres
683 activates subsets of DNA damage and spindle checkpoint pathways in budding
684 yeast yku70Delta mutants. Genes Dev 16**:** 1919-1933.

685 Moser, S. C., S. von Elsner, I. Bussing, A. Alpi, R. Schnabel *et al.*, 2009 Functional
686 dissection of Caenorhabditis elegans CLK-2/TEL2 cell cycle defects during
687 embryogenesis and germline development. PLoS Genet 5**:** e1000451.
688 Musacchio, A., and E. D. Salmon, 2007 The spindle-assembly checkpoint in space and
689 time. Nat Rev Mol Cell Biol 8**:** 379-393.
690 Muzzini, D. M., P. Plevani, S. J. Boulton, G. Cassata and F. Marini, 2008 Caenorhabditis
691 elegans POLQ-1 and HEL-308 function in two distinct DNA interstrand cross-
692 link repair pathways. DNA repair 7**:** 941-950.
693 Neff, M. W., and D. J. Burke, 1992 A delay in the Saccharomyces cerevisiae cell cycle
694 that is induced by a dicentric chromosome and dependent upon mitotic
695 checkpoints. Mol Cell Biol 12**:** 3857-3864.
696 Nitta, M., O. Kobayashi, S. Honda, T. Hirota, S. Kuninaka *et al.*, 2004 Spindle
697 checkpoint function is required for mitotic catastrophe induced by DNA-
698 damaging agents. Oncogene 23**:** 6548-6558.
699 Nystul, T. G., J. P. Goldmark, P. A. Padilla and M. B. Roth, 2003 Suspended animation
700 in C. elegans requires the spindle checkpoint. Science 302**:** 1038-1041.
701 O'Connell, K. F., C. M. Leys and J. G. White, 1998 A genetic screen for temperature-
702 sensitive cell-division mutants of Caenorhabditis elegans. Genetics 149**:** 1303-
703 1321.
704 Palou, R., G. Palou and D. G. Quintana, 2017 A role for the spindle assembly checkpoint
705 in the DNA damage response. Curr Genet 63**:** 275-280.

706 Paques, F., and J. E. Haber, 1999 Multiple pathways of recombination induced by
707 double-strand breaks in Saccharomyces cerevisiae. Microbiology and molecular
708 biology reviews : MMBR 63**:** 349-404.
709 Primorac, I., and A. Musacchio, 2013 Panta rhei: The APC/C at steady state. The Journal
710 of Cell Biology 201**:** 177-189.
711 Roerink, S. F., R. van Schendel and M. Tijsterman, 2014 Polymerase theta-mediated end
712 joining of replication-associated DNA breaks in C. elegans. Genome Res.
713 Scharer, O. D., 2005 DNA interstrand crosslinks: natural and drug-induced DNA adducts
714 that induce unique cellular responses. Chembiochem 6**:** 27-32.
715 Shonn, M. A., R. McCarroll and A. W. Murray, 2000 Requirement of the spindle
716 checkpoint for proper chromosome segregation in budding yeast meiosis. Science
717 289**:** 300-303.
718 Sonneville, R., G. Craig, K. Labib, A. Gartner and J. J. Blow, 2015 Both Chromosome
719 Decondensation and Condensation Are Dependent on DNA Replication in C.
720 elegans Embryos. Cell reports 12**:** 405-417.
721 Stein, K. K., E. S. Davis, T. Hays and A. Golden, 2007 Components of the spindle
722 assembly checkpoint regulate the anaphase-promoting complex during meiosis in
723 Caenorhabditis elegans. Genetics 175**:** 107-123.
724 Tarailo, M., S. Tarailo and A. M. Rose, 2007 Synthetic lethal interactions identify
725 phenotypic "interologs" of the spindle assembly checkpoint components. Genetics
726 177**:** 2525-2530.

Ui, A., M. Seki, H. Ogiwara, R. Onodera, S. Fukushige *et al.*, 2005 The ability of Sgs1 to interact with DNA topoisomerase III is essential for damage-induced recombination. DNA Repair (Amst) 4**:** 191-201.

van Schendel, R., J. van Heteren, R. Welten and M. Tijsterman, 2016 Genomic Scars Generated by Polymerase Theta Reveal the Versatile Mechanism of Alternative End-Joining. PLoS Genet 12**:** e1006368.

Wild, T., M. S. Larsen, T. Narita, J. Schou, J. Nilsson *et al.*, 2016 The Spindle Assembly Checkpoint Is Not Essential for Viability of Human Cells with Genetically Lowered APC/C Activity. Cell Rep 14**:** 1829-1840.

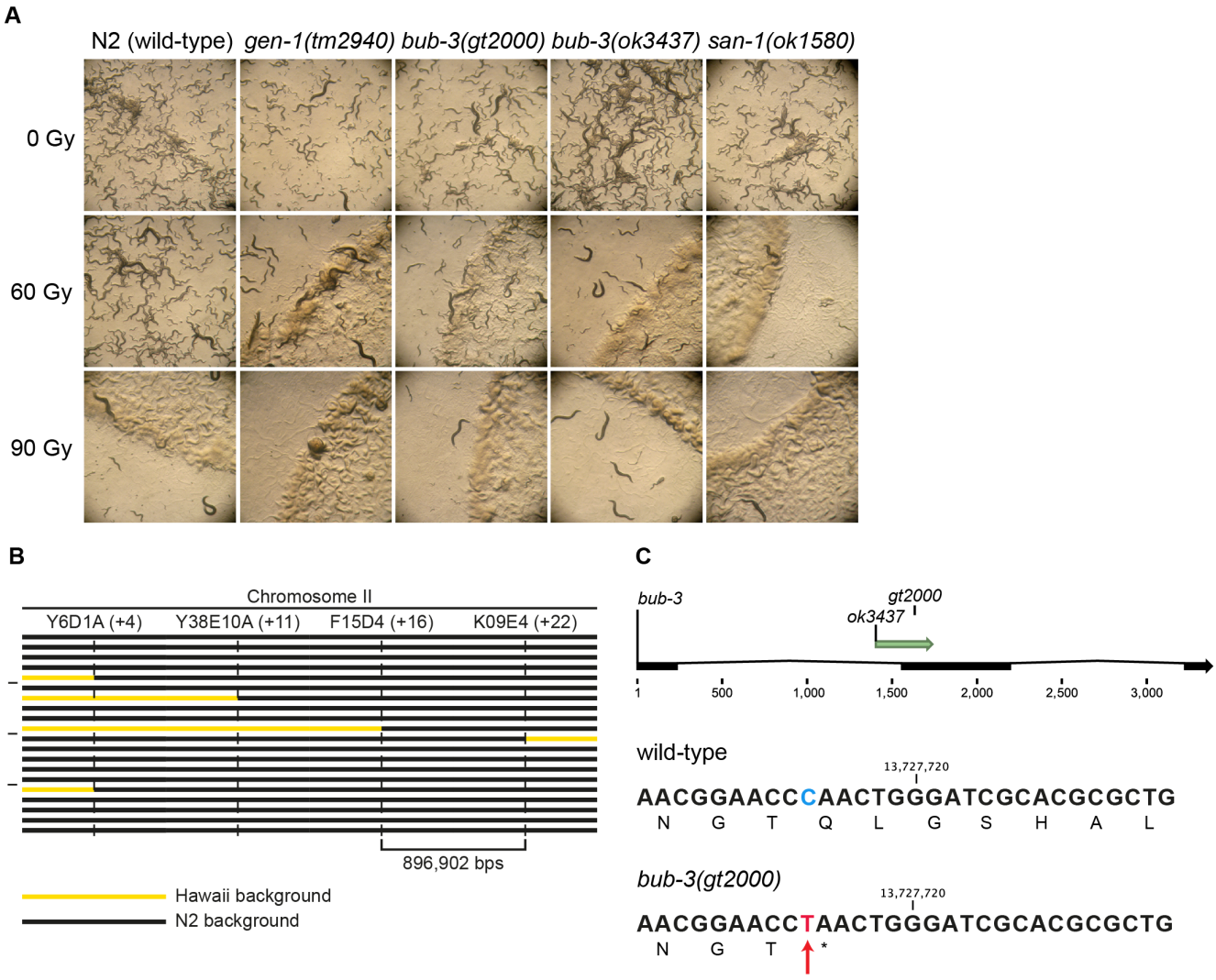
A
N2 (wild-type)
gen-1(tm2940)
bub-3(gt2000)
bub-3(ok3437)
san-1(ok1580)
0 Gy
60 Gy
90 Gy
B
Chromosome II
Y6D1A (+4)
Y38E10A (+11)
F15D4 (+16)
K09E4 (+22)
896,902 bps
Hawaii background
N2 background
C
bub-3
gt2000
ok3437
1
500
1,000
1,500
2,000
2,500
3,000
wild-type
13,727,720
AACGGAACCCAACTGGGATCGCACGCGCTG
N G T Q L G S H A L
bub-3(gt2000)
13,727,720
AACGGAACCTAACTGGGATCGCACGCGCTG
N G T *

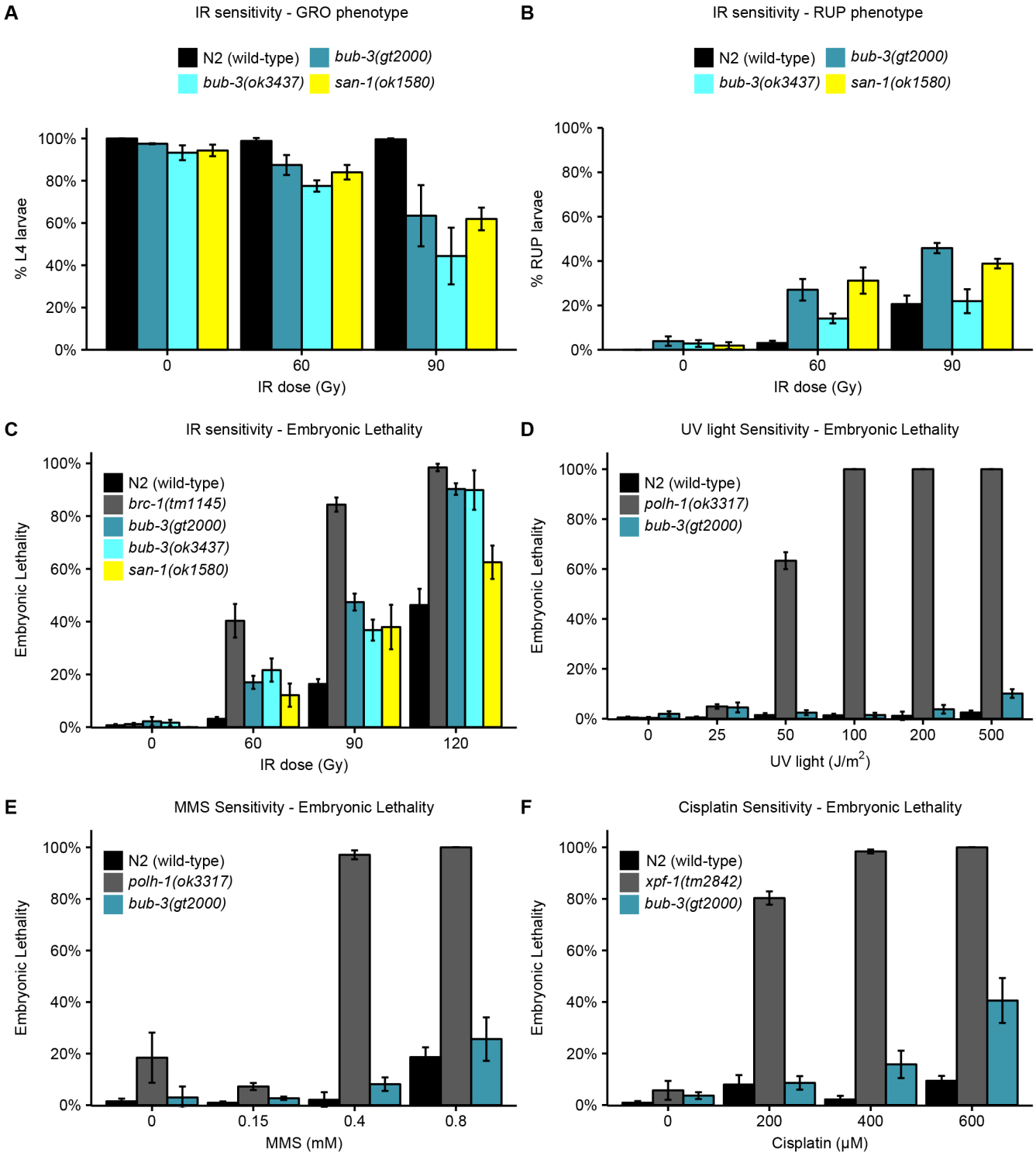
A
IR sensitivity - GRO phenotype
N2 (wild-type)
bub-3(gt2000)
bub-3(ok3437)
san-1(ok1580)
% L4 larvae
100%
80%
60%
40%
20%
0%
0
60
90
IR dose (Gy)
B
IR sensitivity - RUP phenotype
N2 (wild-type)
bub-3(gt2000)
bub-3(ok3437)
san-1(ok1580)
% RUP larvae
100%
80%
60%
40%
20%
0%
0
60
90
IR dose (Gy)
C
IR sensitivity - Embryonic Lethality
N2 (wild-type)
brc-1(tm1145)
bub-3(gt2000)
bub-3(ok3437)
san-1(ok1580)
Embryonic Lethality
100%
80%
60%
40%
20%
0%
0
60
90
120
IR dose (Gy)
D
UV light Sensitivity - Embryonic Lethality
N2 (wild-type)
polh-1(ok3317)
bub-3(gt2000)
Embryonic Lethality
100%
80%
60%
40%
20%
0%
0
25
50
100
200
500
UV light (J/m2)
E
MMS Sensitivity - Embryonic Lethality
N2 (wild-type)
polh-1(ok3317)
bub-3(gt2000)
Embryonic Lethality
100%
80%
60%
40%
20%
0%
0
0.15
0.4
0.8
MMS (mM)
F
Cisplatin Sensitivity - Embryonic Lethality
N2 (wild-type)
xpf-1(tm2842)
bub-3(gt2000)
Embryonic Lethality
100%
80%
60%
40%
20%
0%
0
200
400
600
Cisplatin (µM)

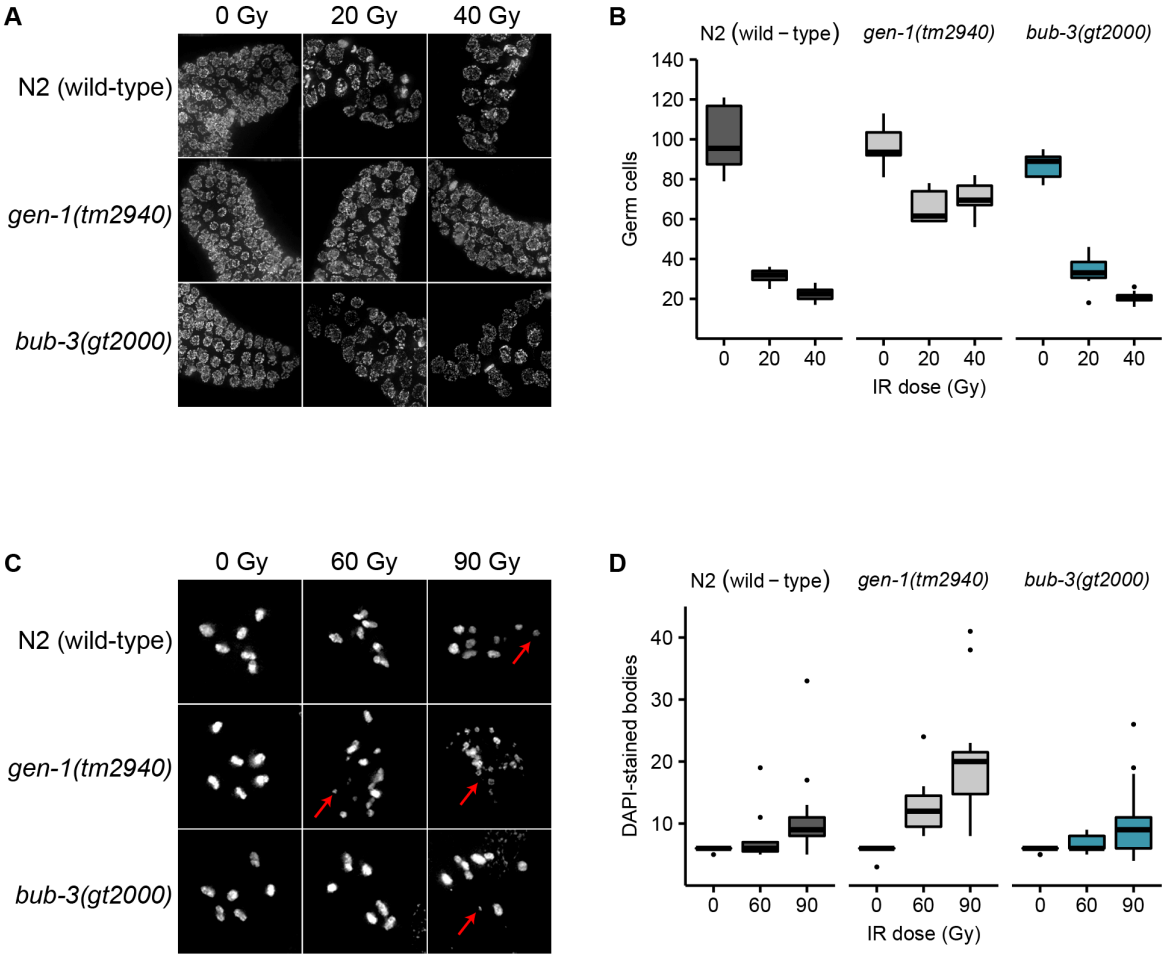
A
0 Gy
20 Gy
40 Gy
N2 (wild-type)
gen-1(tm2940)
bub-3(gt2000)
B
N2 (wild – type)
gen-1(tm2940)
bub-3(gt2000)
Germ cells
140
120
100
80
60
40
20
0
20
40
IR dose (Gy)
C
0 Gy
60 Gy
90 Gy
N2 (wild-type)
gen-1(tm2940)
bub-3(gt2000)
D
N2 (wild – type)
gen-1(tm2940)
bub-3(gt2000)
DAPI-stained bodies
40
30
20
10
0
60
90
IR dose (Gy)

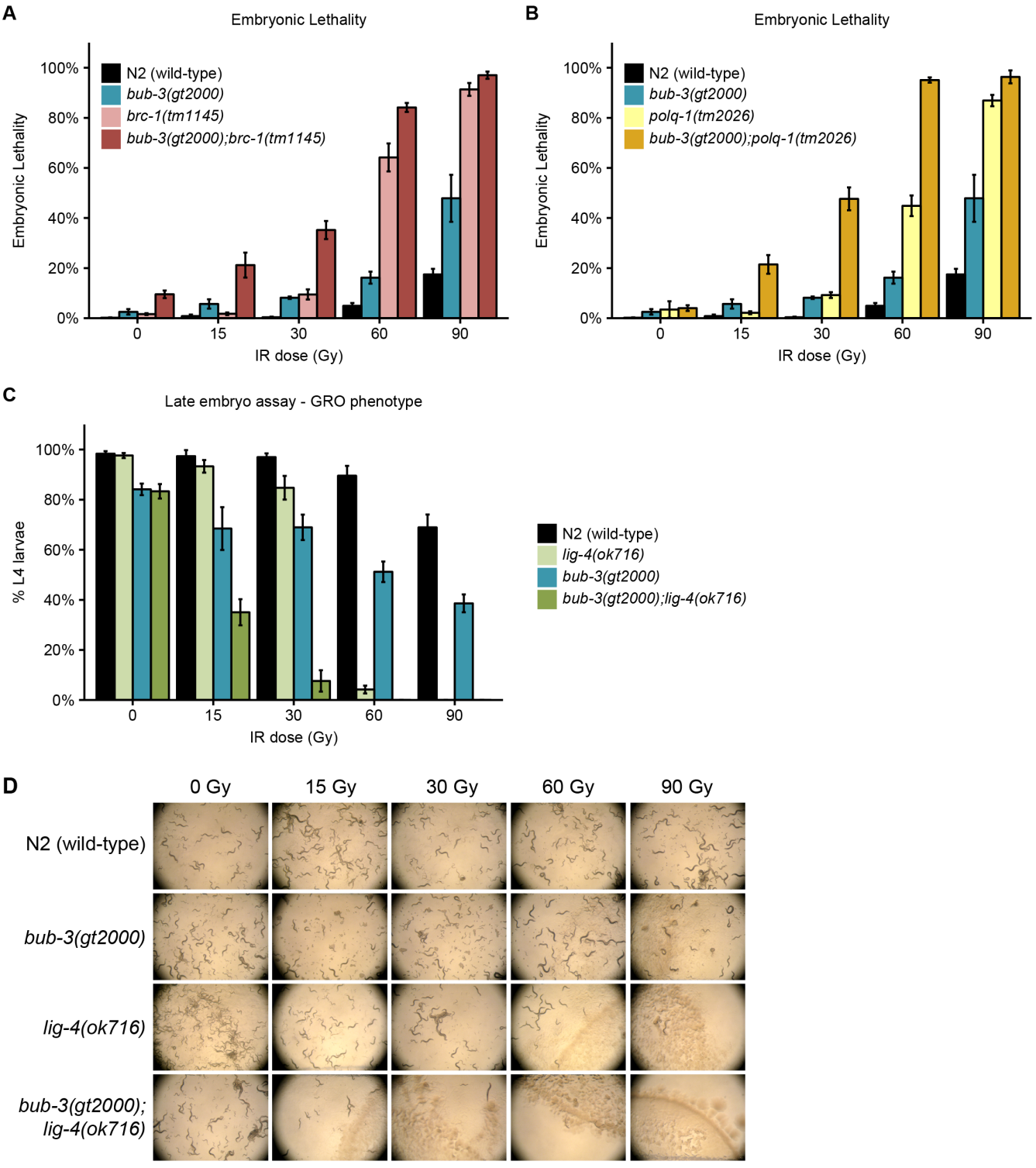
A
Embryonic Lethality
N2 (wild-type)
bub-3(gt2000)
brc-1(tm1145)
bub-3(gt2000);brc-1(tm1145)
Embryonic Lethality
100%
80%
60%
40%
20%
0%
0
15
30
60
90
IR dose (Gy)
B
Embryonic Lethality
N2 (wild-type)
bub-3(gt2000)
polq-1(tm2026)
bub-3(gt2000);polq-1(tm2026)
Embryonic Lethality
IR dose (Gy)
C
Late embryo assay - GRO phenotype
% L4 larvae
N2 (wild-type)
lig-4(ok716)
bub-3(gt2000)
bub-3(gt2000);lig-4(ok716)
IR dose (Gy)
D
0 Gy
15 Gy
30 Gy
60 Gy
90 Gy
N2 (wild-type)
bub-3(gt2000)
lig-4(ok716)
bub-3(gt2000);
lig-4(ok716)

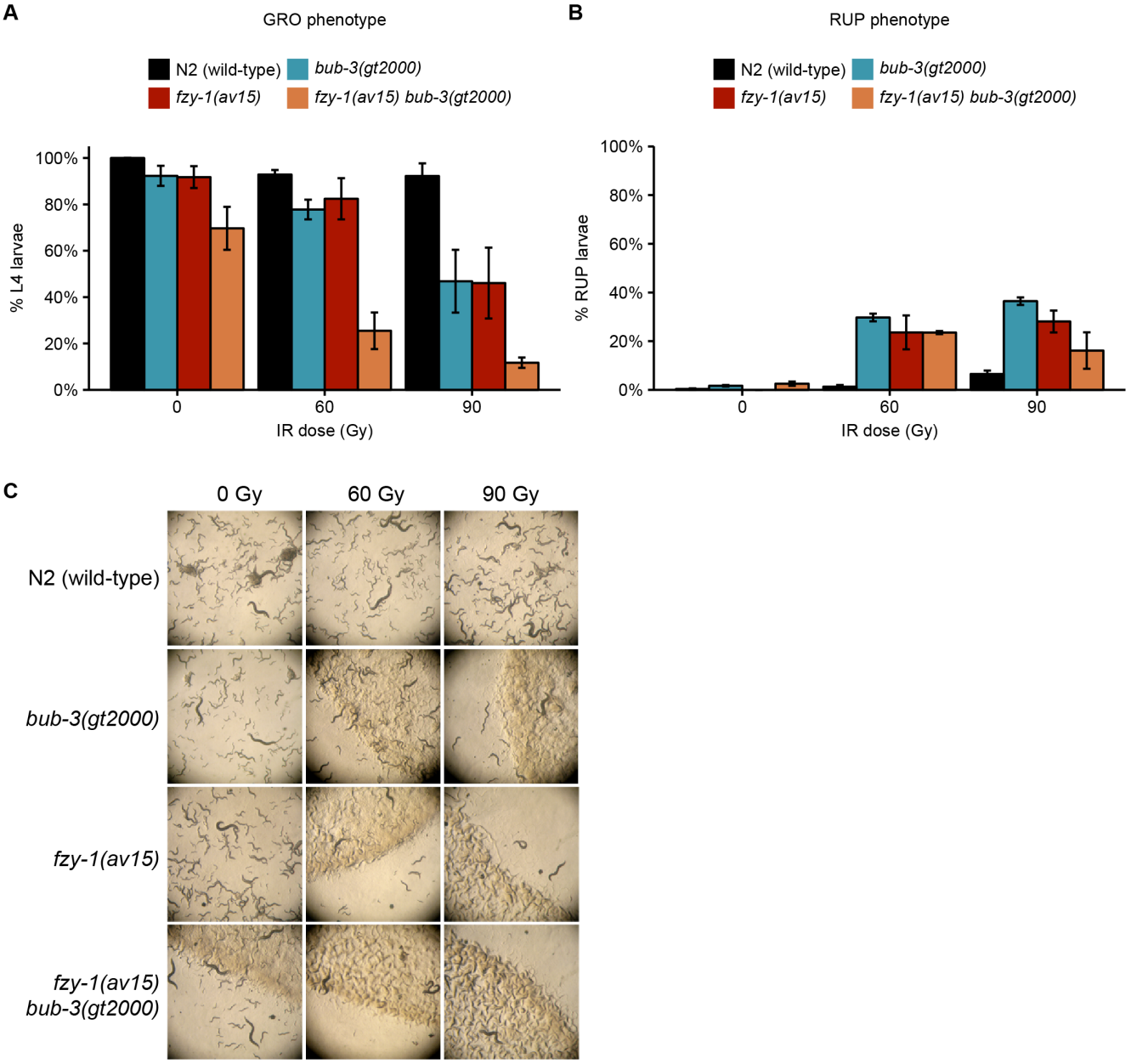
A
GRO phenotype
N2 (wild-type)
bub-3(gt2000)
fzy-1(av15)
fzy-1(av15) bub-3(gt2000)
% L4 larvae
100%
80%
60%
40%
20%
0%
0
60
90
IR dose (Gy)
B
RUP phenotype
N2 (wild-type)
bub-3(gt2000)
fzy-1(av15)
fzy-1(av15) bub-3(gt2000)
% RUP larvae
100%
80%
60%
40%
20%
0%
0
60
90
IR dose (Gy)
C
0 Gy
60 Gy
90 Gy
N2 (wild-type)
bub-3(gt2000)
fzy-1(av15)
fzy-1(av15)
bub-3(gt2000)